RSC Advances

ARTICLE

Effective new method for synthesizing Pt and $CoPt_3$ mesoporous nanorods. New catalysts for ethanol electro-oxidation in alkaline medium.

hReceived 00th January 20xx,
Accepted 00th January 20xx

DOI: 10.1039/x0xx00000x

www.rsc.org/

A. Serrà [a], E. Gómez [a], M. Montiel [b] and E. Vallés [a,*]

In this work, an electrochemical methodology consisting of electrodeposition in ionic liquid-in water (IL/W) microemulsions has been revealed as an excellent pathway to prepare highly mesoporous nanorods with pore sizes of a few nanometers, with a significant growth rate. The nanochannels of a polycarbonate membrane (hard template) define the diameter of the nanorods, the deposited charge controls its length and the mesoporous structure replicates the structure of the microemulsion (soft template). This procedure has been used to prepare mesoporous nanorods of pure metal (Pt) or of alloy ($CoPt_3$) with very high electrochemically active surface area (228 and 235 $m^2\ g^{-1}$, respectively), as a consequence of the accessible three-dimensional interconnected network formed by the mesopores. When the synthesised mesoporous nanorods were tested as catalysts for ethanol electrooxidation in alkaline medium, excellent catalytic performance was found, with significant improvements over the performance of compact nanorods or commercial PtRu nanoparticles. The oxidation current / mass ratio of the mesoporous nanorod catalyst is significantly higher and, moreover, the onset potential of the ethanol oxidation is clearly advanced. Mesoporous $CoPt_3$ nanorods show similar performance with pure platinum mesoporous nanorods and good stability in the alkaline medium, which makes them very good candidates as catalysts of the anodic reaction in direct ethanol fuel cells, with greater economy with respect to pure Pt catalysts.

Introduction

Metallic mesoporous nanostructures have attracted much interest as a consequence of their unique chemical and physical properties (low density, high surface area and high porosity, amongst others). These nanostructures are very useful materials in a broad range of applications, such as in battery electrodes and in fuel cells [1-3], but their performance is still insufficient to meet current high power and high energy density demands [4-6]. In the past two decades, there has been great interest in developing facile, green and scalable synthesis pathways for the preparation of advanced metallic mesoporous nanostructures that have high specific power and volumetric energy density, and high stability [7-9]. Various new electrosynthetic approaches have been investigated along these lines, based on electrodeposition in soft-template systems such as micelle solutions [10-11], liquid crystals [12] and microemulsions [13, 14]. However, as a consequence of the inherent high viscosity of some of these systems, especially lipotropic liquid crystals and some microemulsions, they cannot be applied as a general electrochemical pathway for the shape-controlled synthesis of some nanostructures such as nanorods. When soft-template systems are used as electrodeposition media for the electrochemical synthesis of mesoporous nanostructures in the interior of hard templates, two conditions are necessary: the electrochemical medium must have sufficient fluidity to accede to the nanochannels of the templates, and the structure of the soft template must persist in the nanochannels, in order to define different type of mesoporous nanodeposits [13, 15-17].

Recently, microemulsions containing ionic liquids have been proposed as interesting electrodeposition media for synthesising mesoporous structures. However, depending on the composition of the microemulsions, the method has significant limitations such as low efficiency and low deposition rate [13, 14]. To overcome these limitations, increasing efforts have recently been devoted to establishing better conditions and new microemulsions with ionic liquids that allow these electrodeposition systems to be generalised for the synthesis

[a] Grup d'Electrodeposició de Capes Primes i Nanoestructures (GE-CPN), Departament de Química Física and Institut de Nanociència i Nanotecnologia (IN²UB), Universitat de Barcelona, Martí i Franquès 1, E-08028, Barcelona, Catalonia, Spain.

[b] Departamento de Química Física Aplicada, Universidad Autónoma de Madrid, Francisco Tomás y Valiente 7, 28049, Madrid, Spain.

† Footnotes relating to the title and/or authors should appear here.

of different mesoporous nanomaterials. Moreover, if electrodeposition in microemulsions is combined with the use of hard templates to grow nanostructures, mesoporous nanorods or nanowires can be obtained in a relatively simple way i.e. a shape-controlled synthesis of mesoporous structures will be achieved [10-14]. Furthermore, microemulsions containing ionic liquids have significant advantages as soft templates in comparison with the micellar solutions or liquid crystals that have been proposed by other authors, as a consequence of the unique features of ionic liquids in microemulsions [18-21]. The electroactive species can be dissolved in water and this aqueous solution (W) could be used to form a microemulsion of the ionic liquid in water (IL/W), stabilised by a specific surfactant [22]. These microemulsions present enough conductivity to allow the electrodeposition process to take place at a significant rate, and the selection of different aqueous solutions for the microemulsions could allow the preparation of mesoporous materials of different composition. It has been found that using IL/W microemulsions, the rate, efficiency and viability of the electrodeposition is dramatically increased compared with the inverse microemulsions (W/IL), with good pore definition of the mesoporous deposits [13, 14]. According to our previous studies, non-stirring conditions are necessary to maintain the structure of the microemulsion during the deposition process and to obtain mesoporous materials that replicate that structure. Therefore, electrodeposition in IL/W microemulsions can be proposed as an ideal method for shape-controlled synthesis of mesoporous structures for applications in adsorption, catalysis, electrochemistry and in sensors. Accordingly, herein we report a facile and rapid shape-controlled synthesis of mesoporous Pt and $CoPt_3$ nanorods by means of an electrochemical method. Ionic liquid-in-water microemulsions (soft template) were used as electrochemical media to define porous morphologies, whereas polycarbonate membranes (hard template) were used to define the shape of the nanorods. Moreover, we explore the electrocatalytic activity towards ethanol oxidation in alkaline media of the synthesised mesoporous nanorods, in order to demonstrate their enhanced activity in comparison with compact Pt nanorods or other conventional Pt catalysts. CoPt nanorods are a good material for the catalysis of oxygen reduction in fuel cells and we test if they can also be used as catalysts for the anodic reaction in fuel cells. Moreover, the alkaline medium is less aggressive towards the catalysts than an acidic medium and in this respect ethanol electro-oxidation in alkaline media is a promising chemistry for fuel cells.

Experimental

Materials

Cobalt (II) chloride hexahydrate – $CoCl_2 \cdot 6\ H_2O$, Carlo Erba, > 98.0 %; sodium hexachloroplatinate (IV) hexahydrate – $Na_2PtCl_6 \cdot 6\ H_2O$, Aldrich, 98.0 %; p-octyl poly(ethylene glycol) phenyl ether a.k.a. Triton X-100 – $C_{14}H_{22}O(C_2H_4O)_n$ (n = 9–10), Acros Organics, 98 %; 1-butyl-3-methylimidazolium hexafluorophosphate a.k.a. bmimPF_6 – $C_8H_{15}F_6N_2P$, Solvionic, 99 %; sodium hydroxide – NaOH, Merck, 99%; ethanol – CH_3CH_2OH, Panreac, 99 %; sulphuric acid – H_2SO_4, Sigma, 98 %; PtRu/C – Johnson Matthey, 30 wt. % Pt; and deionised water (Millipore Q-System) with a resistivity of 18.2 MΩ cm^{-1}.

Electrodeposition media. Preparation and physicochemical characterization

Aqueous solutions (W) were used to prepare compact nanorods and ionic liquid-in-water (IL/W) microemulsions to prepare mesoporous nanorods (**Table 1**). The microemulsions (MEs) were prepared by mixing aqueous components (W_1 or W_2), Triton X-100 (S) and bmimPF_6 (IL), in the selected proportions based on the literature (15.1 wt. % of S, 1.1 wt. % of IL and 83.8 % of W) [23]. The mixture was sonicated for 5 min under argon bubbling, leading to transparent and stable microemulsions.

Electrochemical medium				Deposit	
		Composition			Type
Aqueous solutions (W)	W_1	Na_2PtCl_6 20 mM		Pt	Compact NRs
	W_2	Na_2PtCl_6 18 mM + $CoCl_2$ 2 mM		$CoPt_3$	
Ionic liquid-in-water ME (IL/W)	IL/W_1	(wt. %) Triton X-100 (15.1) + BmimPF$_6$ (1.1) + W_i (83.8)	W_1	Pt	Mesoporous NRs
	IL/W_2		W_2	$CoPt_3$	

Table 1: Electrochemical media used to obtain the nanorods with different morphologies.

The physicochemical parameters of each microemulsion such as droplet size, polydispersity index (PI), viscosity and conductivity were determined. Droplet size and polydispersity were analysed by dynamic light scattering (DLS) with Zetasizer Nano ZS (Malvern Instruments) equipment. Electrical conductivity was measured using a Crison conductimeter GLP31 with a 52-92 (Crison) conductivity cell (1 cm^{-1} of cell constant) with a CAT Crison 55-31 temperature sensor with an absolute accuracy of up to ± 0.05 °C. The viscosity measurements of aqueous solutions and microemulsions were performed using an Ostwald viscometer. All measurements were performed in triplicate.

Electrodeposition and characterisation

The electrochemical experiments were carried out using an Autolab microcomputer-controlled potentiostat/galvanostat with PGSTAT30 equipment and GPES software. The voltammetric determination of the optimum range of working potentials in both aqueous and ionic liquid-in-water microemulsions systems was performed at room temperature (25 °C), using a three-electrode electrochemical system. Si / Ti (15 nm) / Au (100 nm) substrates (0.5 x 0.5 cm^2), Pt spiral, and Ag / AgCl / 3M KCl were used as working, counter, and reference electrodes, respectively.

For nanorods preparation, silicon substrates were substituted by polycarbonate (PC) membranes (Millipore) (which act as a hard template in order to define the shape of the nanorods) of 20 µm thickness, 100 nm nominal pore diameter and 10^8 to 2.5 10^9 pores cm^{-2}. Vacuum evaporation was used to coat the membranes with 100 nm of gold on one side (*IMB-CNM*) (1.6 10^{-6} mbar, 6 min, 6.7 kV) to confer conductivity to the membranes. When aqueous solutions were used, the gold coated PC membranes (membranes/Au) were kept in Millipore water for 24 hours prior to the electrodeposition process to make the pores hydrophilic and attain homogeneous growth over the entire membrane. However, when microemulsions were used, the immersion of the membranes/Au in water to fill the channels alters the local composition of the microemulsion, modifying its IL/W structure. Moreover, after 24 h, diffusion and some dissolution of electroactive species in the ionic liquid can occur, avoiding the formation of well-defined mesopores nanorods. Therefore, the PC membranes were used directly with microemulsions, i.e. pores of membrane were not filled with water or microemulsion in order to maintain their soft-template capability; the membranes/Au were contacted with the microemulsions by 15 minutes previous to the electrodeposition process.

The prepared nanorods (NRs) required some etching or cleaning procedures after their synthesis by means of electrodeposition, which consisted of removal of the 100 nm gold layer and dissolving the PC membrane using the following procedure: The Au layer was removed by etching the Au using a saturated solution of I_2/I^-. The PC membranes were dissolved under ultrasonic stirring with chloroform (x5), and then washed with chloroform (x10), ethanol (x5), and Millipore water (x5). NRs were also immersed in 0.1 M NaOH (x3) prior to a final wash in Millipore water before the microemulsions were employed.

The elemental composition was determined using an X-ray analyser incorporated in a Leica Stereoscan S-360 instrument. Nanorod morphology was analysed using field-emission scanning electron microscopy (FE-SEM; *Hitachi H-4100FE*) and high-resolution transmission electron microscopy (HR-TEM; *Jeol 2100*).

In order to determine electrochemical surface area (ECSA) values, suspensions of nanorods in water: ethanol (4: 1) mixtures were dropped onto the surface of glassy carbon electrodes (0.0314 cm^2) and dried under nitrogen flow, resulting in a homogenous coating of catalyst. The ECSA values of the nanorods were obtained by integrating the charge associated with the adsorption and desorption of hydrogen atoms in cyclic voltammograms recorded in H_2SO_4 0.5 M at 100 mV s^{-1}.

Electrocatalytic activity

The electrocatalytic activity of the NRs was evaluated in 1 M NaOH and 1 M CH_3CH_2OH solutions at room temperature. The three-electrode cell consisted of Ag / AgCl / 3M KCl, Pt, and glassy carbon with catalyst electrodes, as the reference, counter, and working electrodes, respectively. Before each electrochemical test, the working electrode was kept in an Ar-saturated 1 M NaOH solution, cycling the potential from 0.2 to −0.9 V at a sweeping rate of 100 mV s^{-1} until reproducible results were obtained. Thereafter, ethanol electrolyte was added and cyclic voltammogram tests were carried out for ethanol oxidation from 0.4 to −0.9 V at a sweeping rate of 50 mV s^{-1}.

Results and Discussion

Synthesis and characterisation of nanorods

Compact and mesoporous nanorods were electrochemically grown inside the pores of polycarbonate membranes (hard template) using different electrochemical media. For electrodeposition of mesoporous nanorods with high pore density IL/W microemulsions (soft template) in non-stirring conditions were used for the plating process (depicted in Fig 1a). Therefore, this electrosynthesis procedure was based on the electrodeposition of metallic ions dissolved in aqueous component (continuous medium) while the ionic liquid droplets define the porous structure. The size of the droplets and its polydispersitivity (**Table 2**) must be related to the size of the mesopores.

Electrochemical medium	Conductivity / mS cm^{-1}	Viscosity / mPa s^{-1}	Droplet size / nm	Polydispersitivity index
W_1	4.9	1.4	-	-
W_2	5.1	1.4	-	-
IL/W_1	3.2	36.5	9.1	0.09
IL/W_2	3.0	36.4	8.9	0.10

Table 2: Physicochemical parameters of each electrochemical medium.

In order to select the optimum range of working potentials, prior to the growth of nanorods, a voltammetric study of both electrochemical media was performed on Si / Ti (15 nm) / Au (100 nm) substrates (0.5 x 0.5 cm^2). As can be seen in Fig. 1b and 1c, both electrochemical media show similar voltammetric profiles for each aqueous solution. However, in the case of the microemulsion media, the current densities were slightly lower as a result of their lower conductivity and relatively higher viscosity (**Table 2**) compared with aqueous solutions (although the viscosity was low enough to fill the pores of polycarbonate membranes), and the intrinsic nature of the IL/W microemulsion structure [24]. Different cathodic limits were used in order to attain a better identification of each voltammetric peak. Bibliographic information [25, 26] and specific experiments were considered when identifying the peaks. Voltammetric profiles with a cathodic limit of −1.2 V allowed the detection of all of the redox processes corresponding to both

systems. This permitted the assignation of platinum deposition from the four different baths, which begins during the first reduction peak (R_1), and is followed by the reduction of Pt and protons over the first deposited Pt (R_2). Moreover, these peaks were detected at different positions as a consequence of the different bath compositions and pH conditions (2.3 and 2.5 for W_1 and W_2, respectively). In the anodic scan, the oxidation of molecular hydrogen adsorbed over the electrode was detected (O_1 in Fig. 1c), except when the anodic scan was recorded under stirring conditions (to detach the hydrogen), even after a hold in the R_2 zone to favour hydrogen evolution. The electrodeposited Pt was detected from its superficial oxidation peak (O_2) at potentials more positive than 500 mV. The reduction of the superficial platinum oxides was clearly seen in the backward scan (R_3). The intensity of these peaks (O_2 and R_3) is indicative of the amount of platinum metal deposited on the electrode.

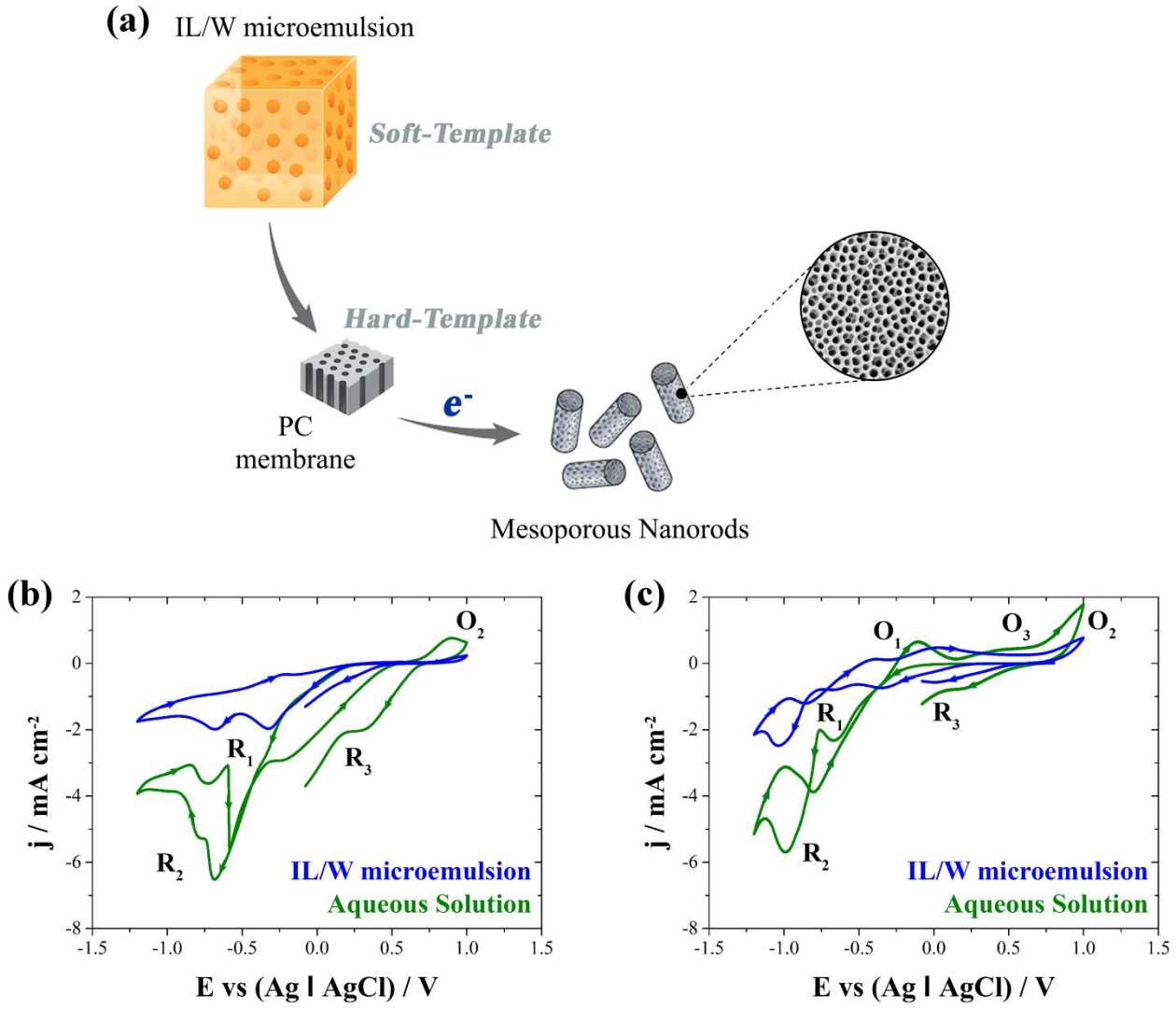

Fig. 1: (a) Schematic representation of the synthesis route of mesoporous nanorods. Cyclic voltammetry under stationary conditions at 50 mV s^{-1} of (b) Pt (IV) and (c) Co(II)-Pt(IV) systems on Si / Ti (10 nm) / Au (100 nm) substrate.

On the other hand, when CoPt solution was used, a similar voltammetric profile was obtained for the initial platinum reduction process, but now cobalt reduction also took place from the potentials of the reduction peak R_2 [27]. Oxidation of the CoPt alloy was detected in the anodic peak O_3, a peak that increased after a hold in the potentials of the reduction peak R_2 and recording the anodic scan in stirring conditions to remove adsorbed molecular hydrogen. Therefore, to obtain a CoPt deposit, sufficiently negative potentials were necessary to avoid the formation of a pure platinum deposit, whereas platinum could be deposited at low negative potentials, to minimise simultaneous hydrogen evolution.

Accordingly, the deposition of Pt and CoPt nanostructures was carried out at fixed potentials of −200 and −1000 mV, respectively.

Fig. 2A-C shows representative FE-SEM images, in which the morphology and structure uniformity of prepared nanorods is presented. However, mesoporous morphology was better displayed in Fig. 2a-c (representative HRTEM images of compact and mesoporous nanorods of Pt and CoPt). Flat lateral surface and no surface defects was observed for the compact nanorods, which demonstrates the good and complete filling of the membranes' channels during the electrodeposition process. Mesoporous nanorods filled also the membranes' channels, with a uniform but porous surface. The ionic liquid does not chemically attack the Pt or CoPt nanorods and, therefore, the observed morphology is a consequence of the pores defined by the droplets of the microemulsion. The EDS analysis of the CoPt nanorods shows that both compact and mesoporous corresponded to the stoichiometry $CoPt_3$. Therefore, microemulsions permit the growth of mesoporous nanorods in a facile manner. Figs. 2b and d show the pore size distributions obtained by measuring the pore size in the TEM images. These results indicate that the average pore size of Pt and $CoPt_3$ nanorods were 3.8 and 3.1 nm, respectively, which confirms superficial porosity. As can be seen, the average pore size was slightly smaller than the hydrodynamic droplet size, which is not surprising as the pores were defined by the size of the ionic liquid droplets, which should be smaller than the hydrodynamic diameter.

Moreover, volumetric porosity must be verified by comparing the electrochemical surface areas of both compact and mesoporous nanorods and of other state-of-the-art mesoporous structures. The obtained nanorods are straight and are highly uniform in terms of length and diameter. The similar length of the compact and mesoporous nanorods synthesised at the same deposition charge reveals that the efficiency of the electrodeposition is similar for both aqueous solutions and microemulsions. However, as could be predicted from the voltammetry experiments, the growth rate of the nanorods clearly decreased in the case of the IL/W microemulsions, changing from 5.1 (W_1)/ 16.6 (W_2) to 1.6 (IL/W_1)/5.2 (IL/W_2) nm s^{-1} due to their different conductivity, viscosity and other properties. It is important to note that the length of all of the nanorods was in the range 3.2 to 3.7 µm. The diameters of the obtained nanorods were 106 ± 9 nm, with a dispersion of values that is a consequence of the non-uniformity of the nanochannels of the PC membrane. Moreover, clear lattice fringes could be observed in all of the micrographs (Fig. 2), with a crystal lattice spacing distance of 0.227 nm for Pt nanostructures, which corresponds to the (111) crystal planes of Pt and 0.229, 0.234 or 0.226 nm for $CoPt_3$ nanostructures, which corresponds to the (111) crystal planes of Pt distorted by the presence of cobalt in the lattice.

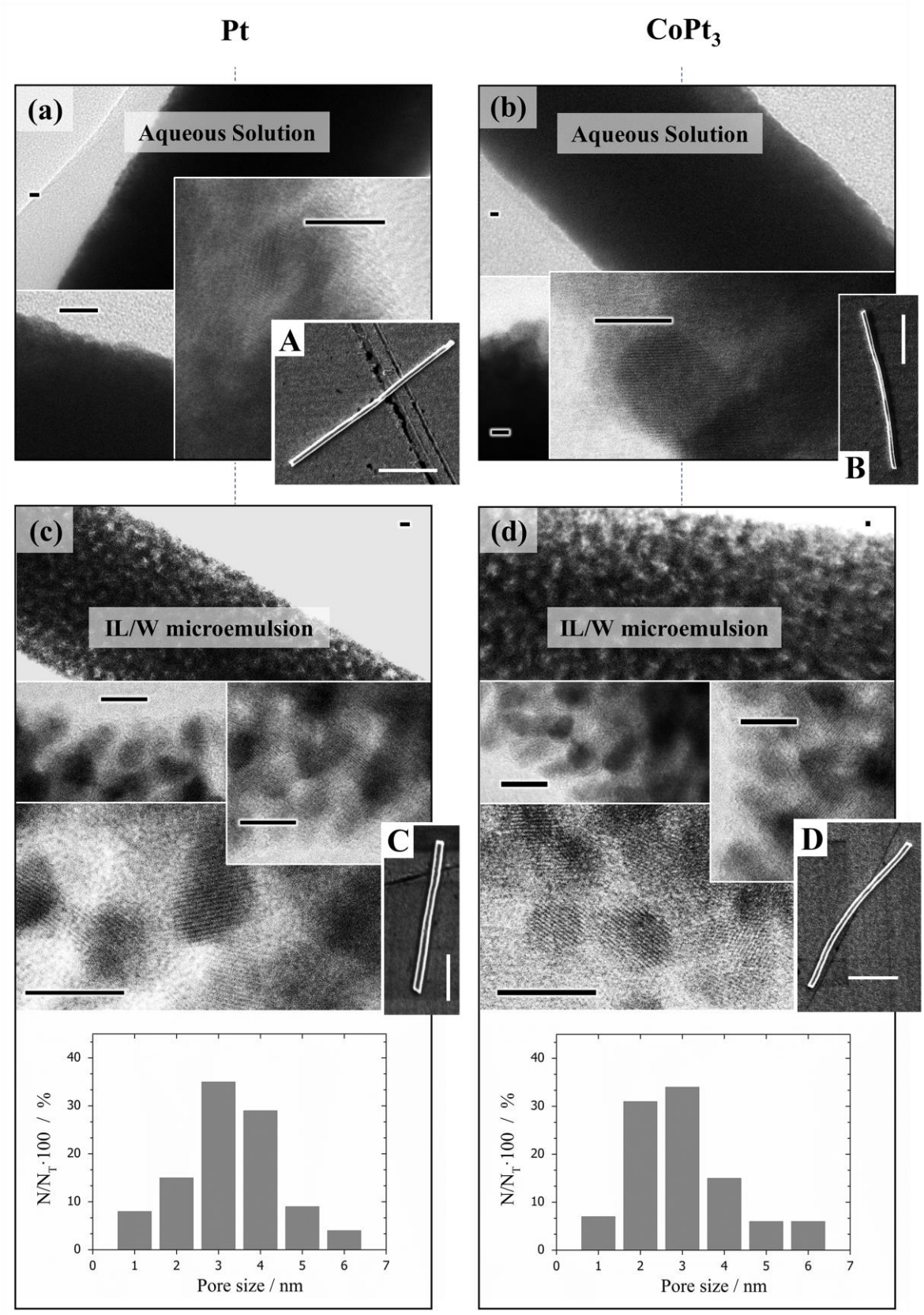

Fig. 2: Transmission electron (a-d) and field-emission scanning (A-D) micrographs of Pt and $CoPt_3$ nanorods prepared in (a, b) aqueous solution (W) or (c, d) ionic liquid-in-water (IL/W) microemulsions. Pore size distribution was also plotted for mesoporous nanorods. Scale bars: 5 nm (black) or 1 µm (white).

The electrochemically active surface areas (ECSAs) were estimated by integrating the voltammograms corresponding to the hydrogen adsorption/desorption from the catalyst surface (Fig. 3). The ECSA values for compact Pt and $CoPt_3$ nanorods were estimated to be 13 and 16 $m^2 g^{-1}$, whereas for mesoporous Pt and $CoPt_3$ nanorods they were 228 and 235 $m^2 g^{-1}$, respectively. As might be expected on observation of the structure of the mesoporous nanorods (those prepared in IL/W microemulsion), they exhibit around 15 times as much surface area as compact nanorods. Moreover, mesoporous nanorods exhibit similar or higher values compared to those of the recent state-of-the-art Pt-based nanostructures [27-30], structures that are useful as catalysts for the electrochemical oxidation of ethanol. Therefore, the formation of a 3D interconnected network, i.e. volumetric porosity, could be assumed based on these comparisons.

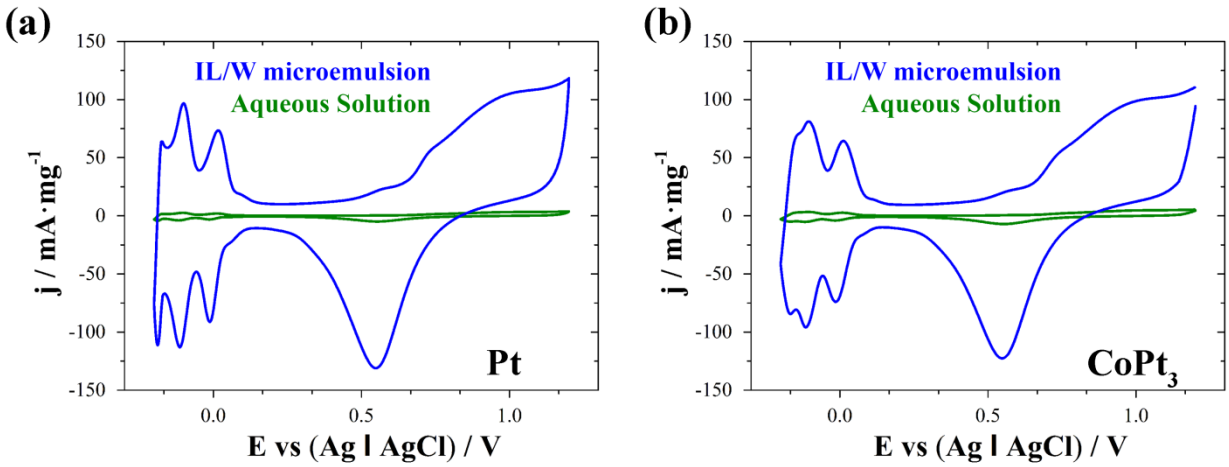

Fig. 3: Cyclic voltammetry (first cycle) of (a) Pt and (b) $CoPt_3$ nanorods in 0.5 M H_2SO_4 solutions at room temperature at a scan rate of 100 mV s^{-1}.

Electrocatalytic activity in alkaline media

To evaluate the electrocatalytic activity of these catalysts for ethanol electrooxidation, cyclic voltammograms of the four types of synthesised nanorods and a commercial PtRu/C catalyst were recorded in 1 M NaOH and 1 M CH_3CH_2OH solutions at room temperature. The currents were normalised by the mass of catalyst. As expected, two well-defined oxidation peaks ascribed to the oxidation of the freshly chemisorbed species coming from the ethanol adsorption (forward scan) and to the removal of the incompletely oxidised carbonaceous species formed during the forward scan (reverse scan) could be clearly identified (Fig. 4). The oxidation signal during the forward scan is usually used to evaluate the catalytic activity of the materials [31, 32]. Ethanol oxidation starts at potentials above −0.70 V for compact nanorods and the current increases with the potential to reach a maximum value at around −0.30 V. However, the ethanol oxidation reaction using mesoporous materials is even more favoured, and the onset potentials are shifted to −0.80 (Pt) and −0.82 V ($CoPt_3$), closer to that of the commercial PtRu/C sample (−0.88 V). Moreover, the slope of the j-V curves is steeper, so the current densities that can be reached using mesoporous materials at low overpotential are higher than those for compact nanorods. Besides the advantages observed at low potentials, mesoporous nanorods of both Pt and $CoPt_3$ composition exhibit the highest mass-normalised current density (1023 and 1073 mA mg^{-1} for Pt and $CoPt_3$, respectively) at similar peak potentials (**Table 3**), as a consequence of the high effective area and the rapidly accessible three-dimensional interconnected network formed by the mesopores. The maximum activity of these catalysts is quite similar and it is five or 3.5 times higher than for compact nanorods (215 and 206 mA mg^{-1} for Pt and $CoPt_3$, respectively) or PtRu/C commercial nanoparticles (303 mA mg^{-1}), respectively.

	Pt / at. %	ECSA / $m^2 g^{-1}$	E_{onset} / V	j_{max} / mA g^{-1}	E_p / V
Compact Pt NRs	100	13	−0.68	215	−0.28
Mesoporous Pt NRs	100	228	−0.80	1023	−0.24
PtRu/C NPs	3	65	−0.88	303	−0.13
Compact $CoPt_3$ NRs	75	16	−0.62	206	−0.35
Mesoporous $CoPt_3$ NRs	75	235	−0.82	1073	−0.26

Table 3: Catalyst characterisation and catalytic performance of different catalysts.

Remarkably, the mass activity of our mesoporous nanorods was also higher than that of previously reported state-of-the-art Pt- or Pd-based nanomaterials such as PdPt alloy nanowires and other catalysts [33-38], indicating that the prepared Pt-based catalyst possesses excellent catalytic activity. Therefore, the enhanced electrocatalytic performance of mesoporous structures can be ascribed to the interconnected porous structure, which can provide

more active sites available for the adsorption of small molecules and promote electron transport during the reaction process.

The antipoisoning properties and durability of our prepared nanorods are vital for their practical applications in fuel cells and were evaluated by chronoamperometric measurements at potentials of −0.4 and −0.6 V for 6000 s (Fig 4c and 4d). As can be seen in chronoamperometric curves in Fig. 4, an initially rapid current decay for all catalysts was observed, probably as a consequence of the accumulations of poisonous carbonaceous intermediates (such as CO_{ads}, ,CH_3CHO_{ads}, amongst others) on the catalyst surface during the ethanol oxidation reaction [36, 37]. Obviously, throughout the measurement process, the current density of ethanol oxidation on mesoporous structures is higher than that on compact nanorods, demonstrating that mesoporous nanorods have greater catalytic activity and better stability for ethanol oxidation compared with compact ones, consistent with the CV results shown in Figs 4a and 4b.

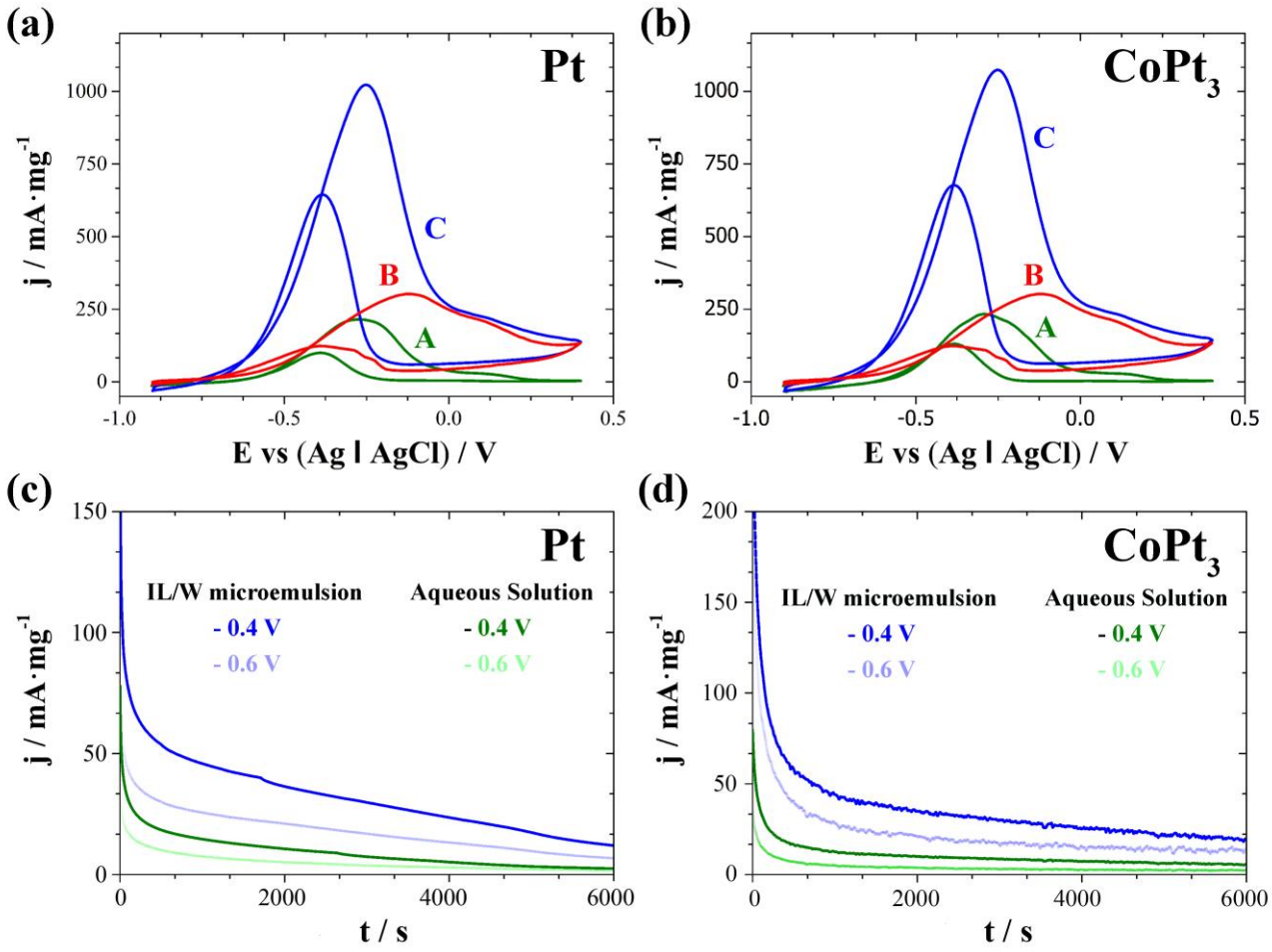

Fig. 4: Cyclic voltammograms at 50 mV s^{-1} of (a) Pt and (b) $CoPt_3$ nanorods, and chronoamperometric curves (recorded at −0.6 or −0.4 V) of (c) Pt and (d) $CoPt_3$ nanorods for methanol oxidation in 1 M NaOH and 1 M CH_3CH_2OH solution.

Conclusions

The electrodeposition of metals and alloys inside the pores of polycarbonate membranes using an ionic liquid-in-water (IL/W) microemulsion, allowed us to synthesise mesoporous nanorods of very high porosity with pore diameters in the 2–4 nm range. The proposed procedure is able to synthesise nanorods of pure metals (such as Pt) or alloys (such as $CoPt_3$), only by controlling the composition of the aqueous component (W) of the microemulsion. The procedure requires the use of IL/W microemulsions with a very low amount of IL in order to maintain a high conductivity of the electrodeposition medium and a significant deposition rate. For the selected microemulsion composition the growth rate of the mesoporous nanorods is only three times lower than that observed for compact nanorods grown in pure aqueous solution, for both the Pt and $CoPt_3$ systems.

The high density of pores and their small size leads to very high ECSA values, implying that the synthesised mesoporous nanorods can be very effective catalysts for induced electrochemical reactions. This is demonstrated in the voltammetry curves of ethanol electrooxidation in alkaline medium on the mesoporous

nanorods supported on vitreous carbon substrates, in which the mass-normalised oxidation peaks show values 5/3.5 times greater than compact nanostructures or commercial PtRu nanoparticles. The prepared $CoPt_3$ mesoporous structures show excellent stability in aggressive acidic or alkaline media, because the effective area of the nanorods is maintained during a high number of voltammetric cycles. This means that $CoPt_3$ nanorods could be used as catalysts in ethanol fuel cells, as an improved alternative to pure Pt or PtRu commercial nanostructures.

Acknowledgements

This work was supported by the EU ERDF (FEDER) funds and the Spanish Government grant TEC2014-51940-C2-2-R from *Ministerio de Economía y Competitividad (MINECO)*. A. Serrà thanks the *Ministerio de Educación, Cultura y Deporte* for a predoctoral grant (FPU). The authors thank the CCiT-UB for the use of their equipment.

References

1 C. Sun, Z. Xie, C. Xia, H. Li, L. Chen, Electrochemistry Communications, 2006, **8**, 833.
2 A. Stein, Advanced Materials, 2003, **15**, 763.
3 H. Chang, S. H. Joo, C. Pak, Journal of Materials Chemistry, 2007, **17**, 3078.
4 M. Yu, J. Chen, J. Liu, S. Li, Y. Ma, J. Zhang, J. An, Electrochimica Acta, 2015, **151**, 99.
5 M .Yang, R. Guarecuco, F. J. Disalvo, Chemistry of Materials, 2013, **25**, 1783.
6 M. M. Bruno, F. A. Viva, M. A. Petruccelli, H. R. Corti, Journal of Power Sources, 2015, **278**, 458.
7 I. I. Slowing, J. L. Vivero-Escoto, C.-W. Wu, V.S.-Y. Lin, Advanced Drug Delivery Reviews, 2008, **60**, 1278.
8 A. Taguchi, E. Schüth, Microporous and Mesoporous Materials, 2005, **77**, 1.
9 M. Hartmann, Chemistry of Materials, 2005, **17**, 4577.
10 C. Li, T. Sato, Y. Yamauchi, Angewandte Chemie – International Edition, 2013, **52**, 8050.
11 C. Li, Y. Yamauchi, Chemistry – A European Journal, 2014, **20**, 729.
12 Y. Yamauchi, A. Tonegawa, M. Komatsu, H. Wang, L. Wang, Y. Nemoto, N. Suzuki, K. Kuroda, Journal of the American Chemical society, 2012, **134**, 5100.
13 A. Serrà, E. Gómez, E. Vallés, International Journal of Hydrogen Energy, 2015, **40**, 8062.
14 A. Serrà, E. Gómez, E. Vallés, Electrochimica Acta, 2015, **174**, 630.
15 G. S. Attard, C. G. Goltner, J. M. Corker, S. Henke, R. H. Templer, Angewandte Chemie – International Edition, 1997, **36**, 1315.
16 O. Corduneanu, V. C. Diculescu, A.-M. Chiorcea-Paquim, A.-M. Oliveira-Brett, Journal of Electroanalytical Chemistry, 2008, **624**, 97.
17 M. Cortés, A. Serrà, E. Gómez, E. Vallés, Electrochimica Acta, 2011, **56**, 8232.
18 H. Gao, J. Li, B. Han, W. Chen, J. Zhang, R. Zhang, D. Yan, Physical Chemistry Chemical Physics, 2004, **6**, 2914.
19 R. Atkin, G. G. Warr, Journal of Physical Chemistry, 2007, **111**, 9309.
20 J. Eastoe, S. Gold, S.E. Rogers, A. Paul, T. Welton, R. K. Heenan, I. Grillo, Journal of the American Chemical Society, 2005, **127**, 7302.
21 J. Piekart, J. Luczak, Soft Matter, 2015, **11**, 8992.
22 M. Moniruzzaman, N. Kamiya, K. Nakashima, M. Goto, Green Chemistry, 2008, **10**, 497.
23 Y. Gao, S. Han. B. Han, G. Li, D. Shen, Z. Li, J. Du, W. Hou, G. Zhang, Langmuir, 2005, **21**, 5681.
24 A. Serrà, E. Gómez, I. V. Golosovsky, J. Nogués, and E. Vallés, Journal of Materials Chemistry A, 2016, **DOI:** 10.1039/C6TA02035F.
25 M. Cortés, E. Gómez, E. Vallés, Electrochemistry Communications, 2010, **12**, 132.
26 S. Grau, M. Montiel, E. Gómez, E. Vallés Electrochimica Acta, 2013, **109**, 187.
27 C. Zhang, H. Yang, T. Sun, N. Shan, J. Chen, L. Xu, Y. Yan, Journal of Power Sources, 2014, **245**, 579.
28 Y. Xu, Y. Han, C. Gao, X. Cao, Nano Energy, 2015, **17**, 111.
29 C. Li, V. Malgras, S. M. Alshehri, J. H. Kim, Y. Yamauchi, Electrochimica Acta, 2015, **183**, 107.
30 Y. Cao, Y. Yang, Y. Shan, C: Fu, N. V. Long, Z. Huang, X. Guo, M. Nogami, Nanoscale, 2015, **7**, 19461.
31 T. Iwasita, X. H. Xia, H. D. Liess, W. Vielstich, journal of Physical chemistry B, 1997, **101**, 7542.
32 C. S. L. Stanley, M. T. M. Koper, Physical Chemistry Chemical Physics, 2009, **11**, 10446.
33 C. Zhu, S. Guo, S. Dong, Journal of Materials Chemistry, 2012, **22**, 1485.
34 C. Xu, P. K. Shen, Y. Liu, Journal of Power Sources, 2007, **164,** 527.
35 S. Ghosh, H. Remita, P. Kar, S. Choudhury, S. Sardar, P. S. Roy, S. K. Bhattacharya, S. K. Pal, Journal of Material Chemistry A, 2015, **3**, 9517.
36 S.-C. Lin, J.-Y. Chen, Y.-F. Hsieh, P.-W. Wu, Materials Letters, 2011, **65**, 215.
37 Z. Y. Huang, H. H. Zhou, F. F. Sun, C.P. Fu, F.Y. Zeng,T. Q. Li, Y. F. Kuang, Y. F. Chemistry – A European Journal, 2013, **19**, 13720.
38 X. M. Chen, X. Chen, M. G. Oymac, Journal of Materials Chemistry A, 2014, **2**, 315.